Supplementary Material: Atomistic Engineering of Ag/Pt nanoclusters for remarkably boosted mass electrocatalytic activity

Liangzhen Liu,[#, 1] Qiang-Yu Zhu,[#, 2, 3] Junwei Li,[1] Junxiang Chen,[1] Junheng Huang,[1] Qing-Fu Sun,*[2], Zhenhai Wen*[1]

[1] CAS Key Laboratory of Design and Assembly of Functional Nanostructures, Fujian Provincial Key Laboratory of Nanomaterials, Fujian Institute of Research on the Structure of Matter, Chinese Academy of Sciences, Fuzhou, Fujian 350002, PR China

[2] State Key Laboratory of Structural Chemistry, Fujian Institute of Research on the Structure of Matter, Chinese Academy of Sciences, Fuzhou, Fujian 350002, PR China

[3] University of Chinese Academy of Science, Beijing 100049, PR China

[#]The authors contribute equally.

***Correspondence to:** wen@fjirsm.ac.cn ; qfsun@fjirsm.ac.cn

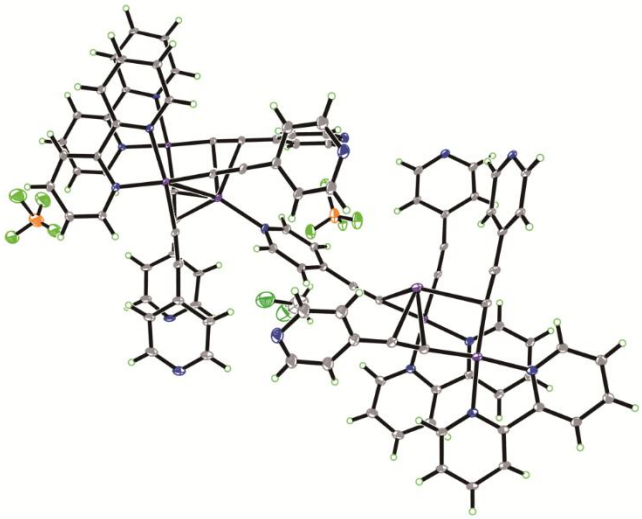

Figure S1. Ortep drawing of the asymmetric unit in the crystal structure of Pt_8Ag_4-MOCs (at 30% probability).

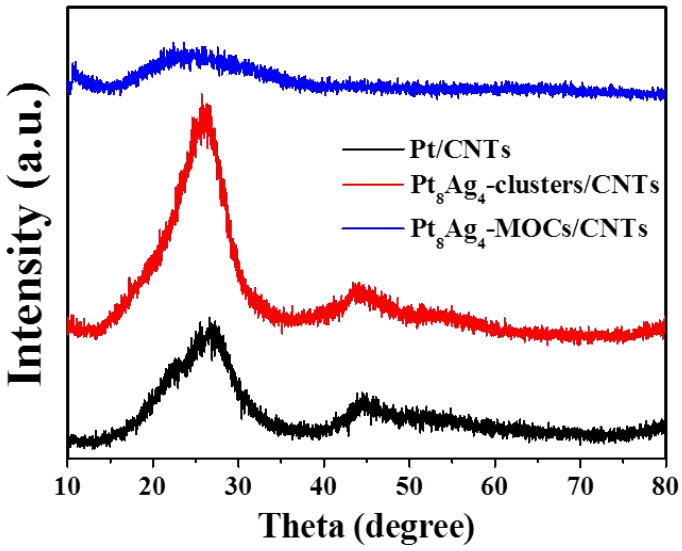

Figure S2. XRD patterns of Pt_8Ag_4-MOCs/CNTs, Pt_8Ag_4-clusters/CNTs and Pt/CNTs.

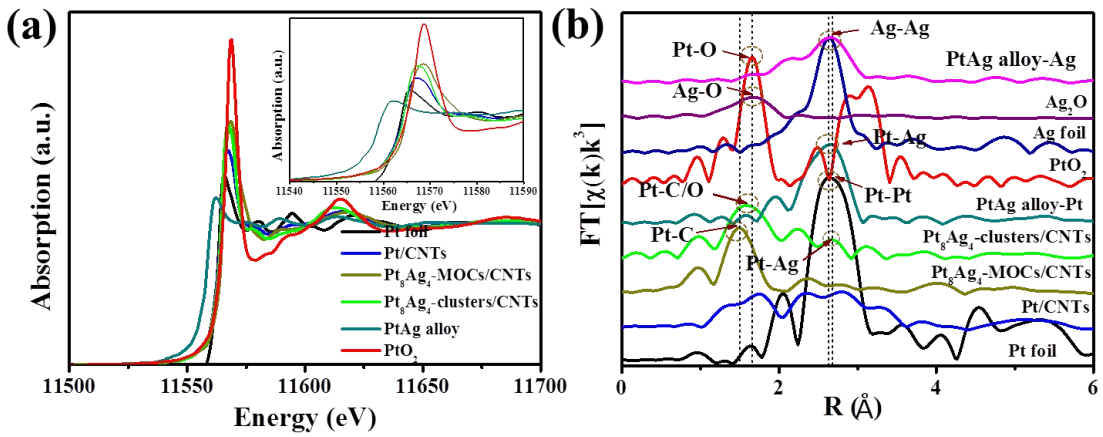

Figure S3. (a) XANES and (b) EXAFS spectra of Pt_8Ag_4-clusters/CNTs, Pt/CNTs, Pt_8Ag_4-MOCs/CNTs, PtAg alloy, PtO_2, Pt foil, Ag_2O and Ag foil.

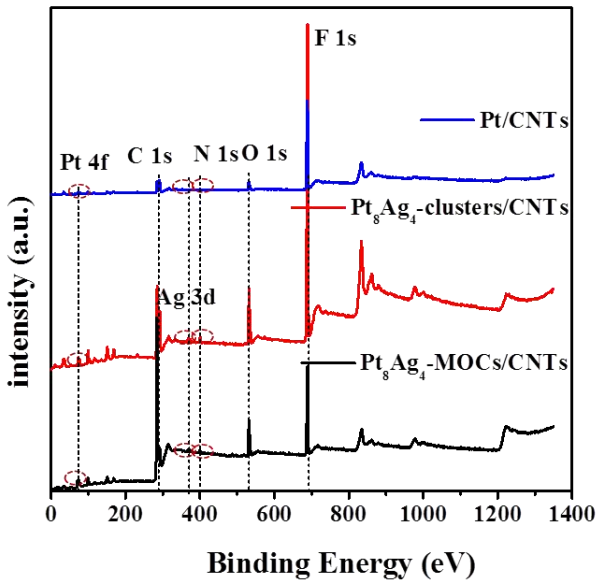

Figure S4. XPS of Pt_8Ag_4-clusters/CNTs, Pt_8Ag_4-MOCs/CNTs and Pt/CNTs.

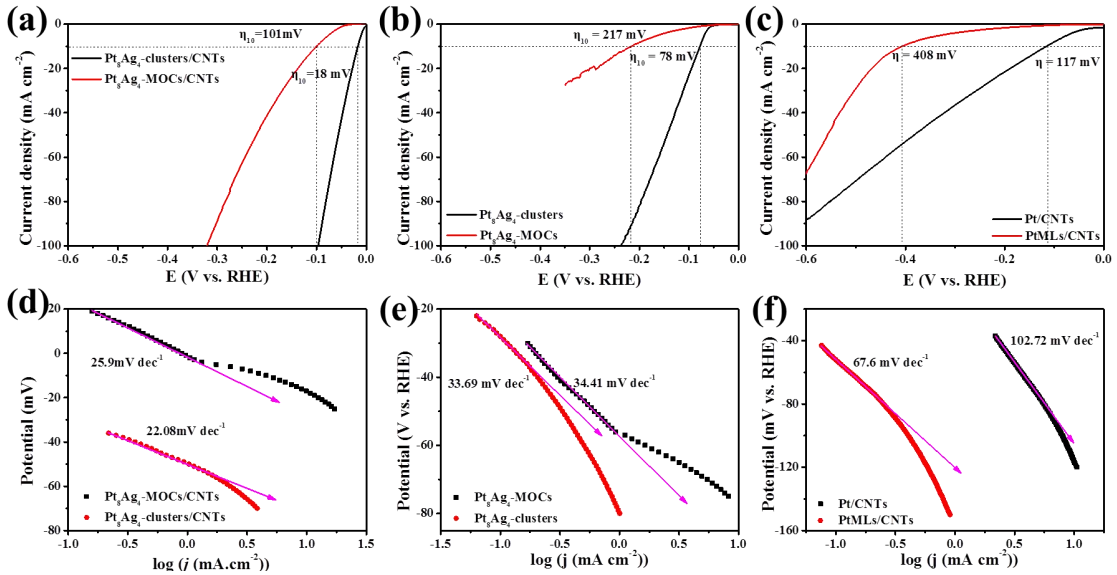

Figure S5. LSV of Pt_8Ag_4-clusters/CNTs and Pt_8Ag_4-MOCs/CNTs (a); Pt_8Ag_4-clusters and Pt_8Ag_4-MOCs (b); Pt/CNTs and PtMLs/CNTs (c) for HER with a sweep rate of 5 mV s^{-1} in 0.5 M H_2SO_4 solution. The Tafel slops of Pt_8Ag_4-clusters/CNT, and Pt_8Ag_4-MOCs/CNTs (d); Pt_8Ag_4-clusters and Pt_8Ag_4-MOCs (e); Pt/CNTs and PtMLs/CNTs (f).

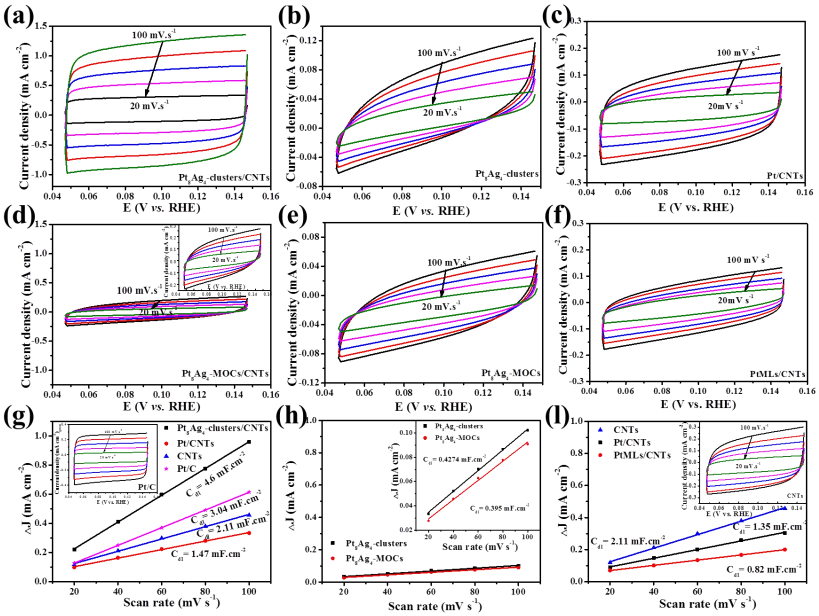

Figure S6. (a-f) The CVs of Pt_8Ag_4-clusters/CNTs, Pt_8Ag_4-MOCs/CNTs, Pt_8Ag_4-clusters, Pt_8Ag_4-MOCs, Pt/CNTs and PtMLs/CNTs with a sweep rate of 5 mV s^{-1} in 0.5M H_2SO_4 solution, respectively (The inset in (d) displays the enlarged view of (d)). The $\triangle J$ of Pt_8Ag_4-clusters/CNTs, Pt_8Ag_4-MOC/CNTs and CNTs (g); Pt_8Ag_4-clusters and Pt_8Ag_4-MOCs (h); Pt/CNTs, PtMLs/CNTs and CNTs (l) plotted against scan rate to the potential of 0.97 V *vs.* RHE (The inset in (l) displays the CVs of CNTs).

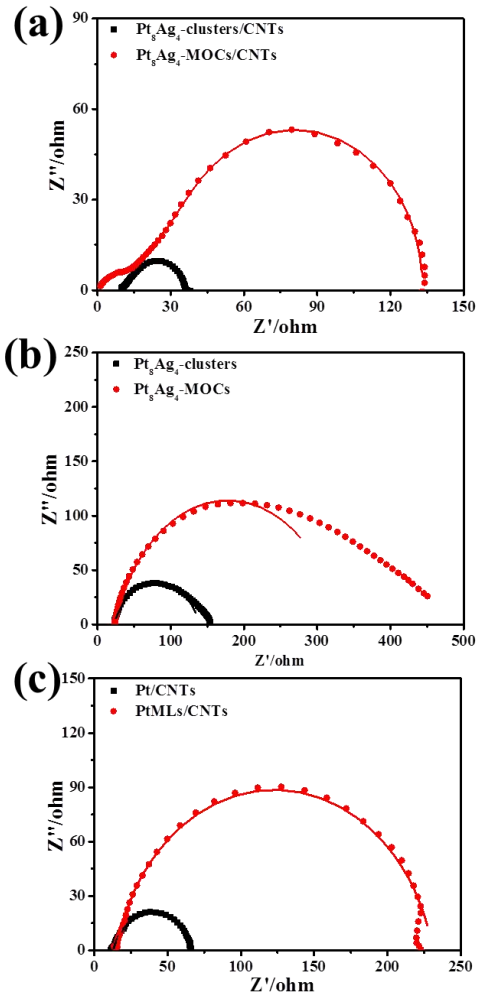

Figure S7. EIS of Pt_8Ag_4-clusters/CNTs and Pt_8Ag_4-MOCs/CNTs (a); Pt_8Ag_4-clusters and Pt_8Ag_4-MOCs (b); Pt/CNTs and PtMLs/CNTs (c) in 0.5 M H_2SO_4 solution at the current density of 10 mA cm^{-2}, respectively.

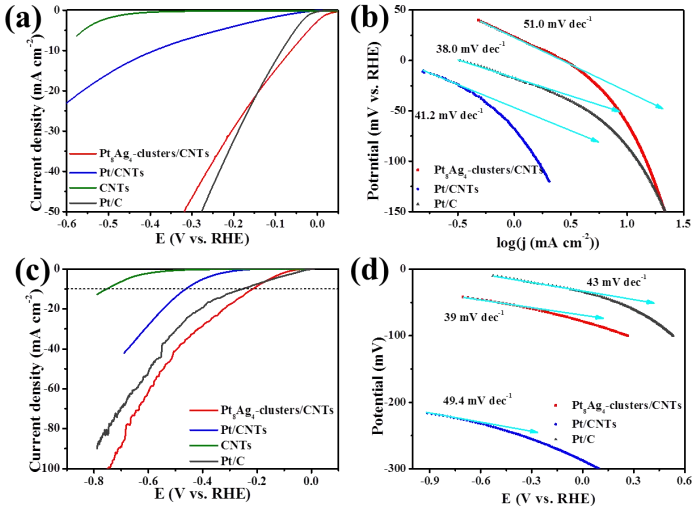

Figure S8. (a) LSV polarization curves of HER at a scan rate of 5 mV s^{-1}; (b) Tafel plots Pt_8Ag_4-clusters/CNTs, Pt/CNTs, CNTs and commercial Pt/C in 1 M KOH solution respectively. (c) LSV polarization curves of HER at a scan rate of 5 mV s^{-1}; (d) Tafel plot of Pt_8Ag_4-clusters/CNTs, Pt/CNTs and commercial Pt/C in 1M PBS solution respectively.

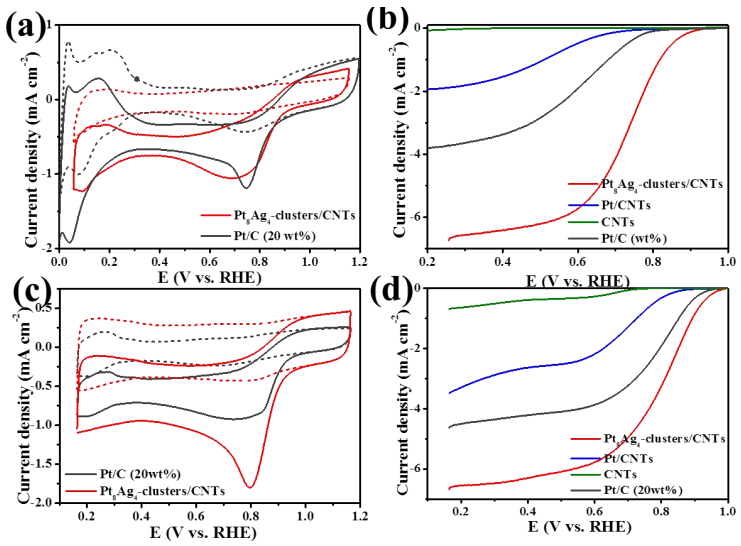

Figure S9. (a) CV curves of Pt_8Ag_4-clusters/CNTs and Pt/C in O_2 or N_2-saturated in 0.1 M KOH solution at a scan rate of 50 mV s^{-1}; (b) the LSV curves of CNTs, Pt_8Ag_4-clusters, Pt_8Ag_4-clusters/CNTs and Pt/C in O_2 saturated 0.1M KOH solution at a scan rate of 5 mV s^{-1} respectively.

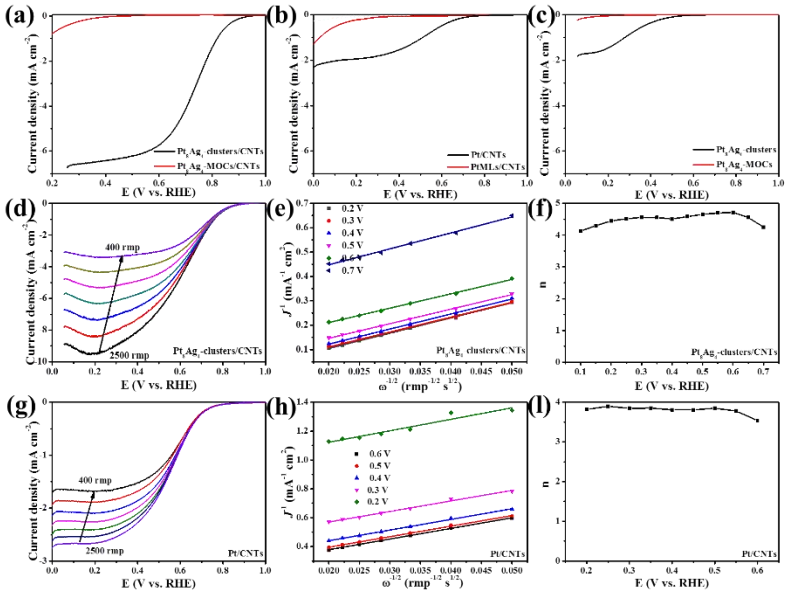

Figure S10. (a-c) RDE polarization curves of Pt_8Ag_4-clusters/CNTs, Pt_8Ag_4-MOCs/CNTs, P Pt_8Ag_4-clusters, Pt_8Ag_4-MOCs, Pt/CNTs and PtMLs/CNTs for ORR with a sweep rate of 5 mV s^{-1} at 1600 rmp; (d) and (g) RDE polarization curves of Pt_8Ag_4-clusters/CNTs and Pt/CNTs at different rotation rates; (e) and (h) the K-L plots of Pt_8Ag_4-clusters/CNTs and Pt/CNTs; (f) and (l) the electron transfer numbers of Pt_8Ag_4-clusters/CNTs and Pt/CNTs based the corresponding K-L plots in O_2-saturated 0.5M H_2SO_4 solution, respectively.

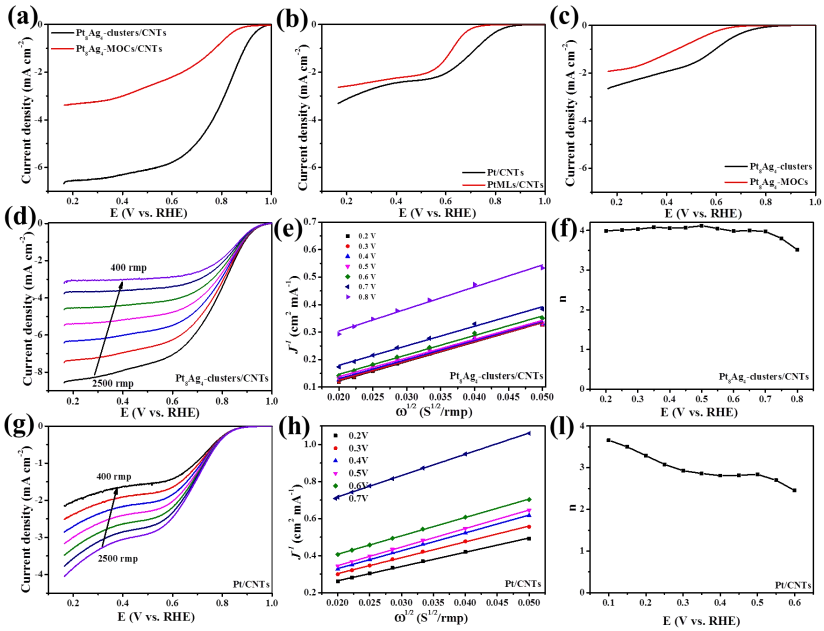

Figure S11. (a-c) RDE polarization curves of Pt_8Ag_4-clusters/CNTs, Pt_8Ag_4-MOCs/CNTs, Pt_8Ag_4-clusters, Pt_8Ag_4-MOCs, Pt/CNTs and PtMLs/CNTs for ORR with a sweep rate of 5mV s^{-1} and 1600rmp; (d) and (g) RDE polarization curves of Pt_8Ag_4-clusters/CNTs and Pt/CNTs at different rotation rates; (e) and (h) the K-L plots of Pt_8Ag_4-clusters/CNTs and Pt/CNTs; (f) and (l) the electron transfer numbers of Pt_8Ag_4-clusters/CNTs and Pt/CNTs based the corresponding K-L plots in O_2-saturated 0.1 KOH solution, respectively.

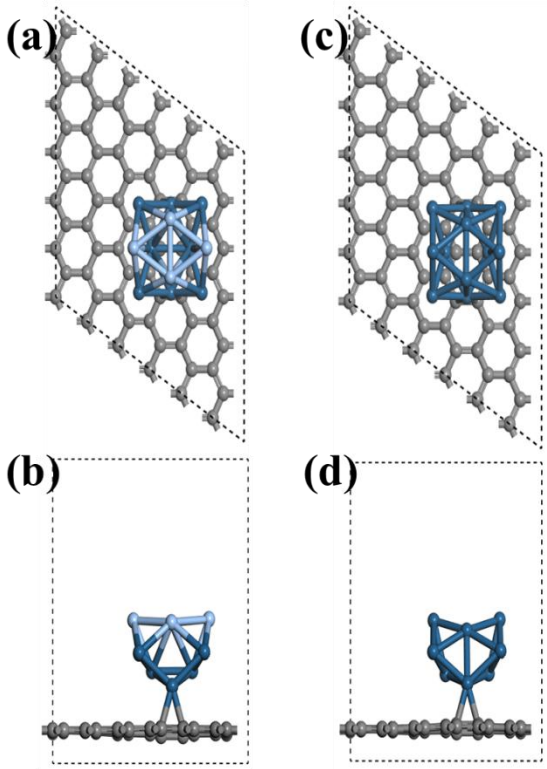

Figure S12. Top (a) and side (b) view of the model of Pt_8Ag_4/CNT and top (c) and side (d) view of the model of Pt/CNT which were used for calculation of HER and ORR. Dark blue, sky blue and grey atoms represent Pt, Ag and C, respectively.

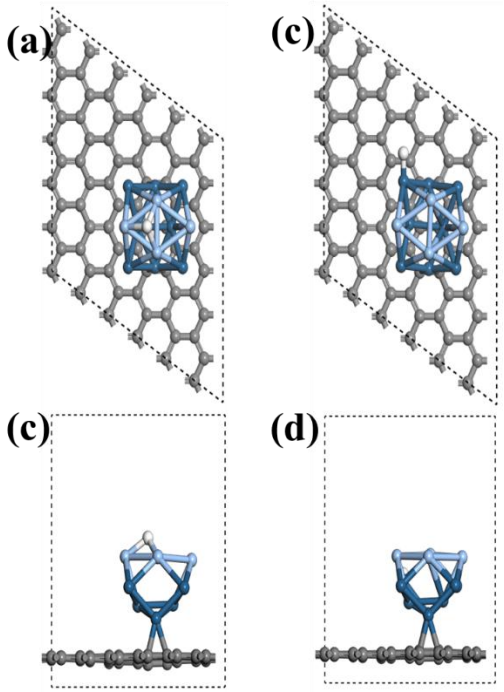

Figure S13. Top (a) and side (b) view of the model of Pt_8Ag_4/CNTand the H atom at the Ag site; Top (c) and side (d) view of the model of Pt_8Ag_4/CNT and the H atom at

the Pt site. Dark blue, sky blue, grey and white atoms represent Pt, Ag, C and H, respectively.

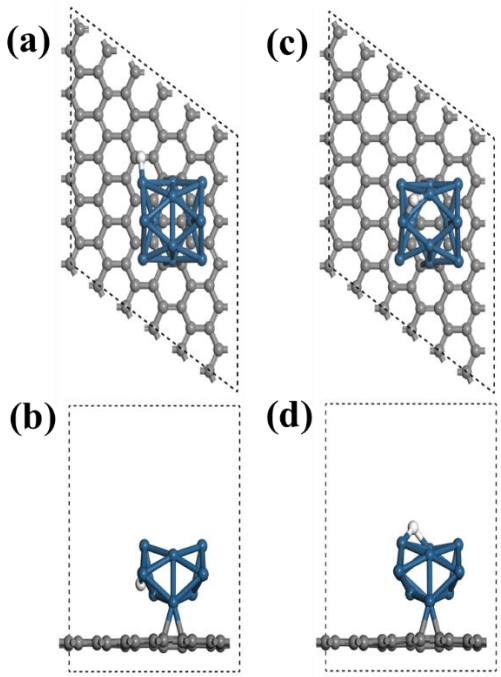

Figure S14. Top (a) and side (b) view of the model of Pt/CNTand the H atom at the top site; and top (c) and side (d) view of the model of Pt/CNT and the H atom at bridge site. Dark blue, sky blue, grey and white atoms represent Pt, Ag, C and H, respectively.

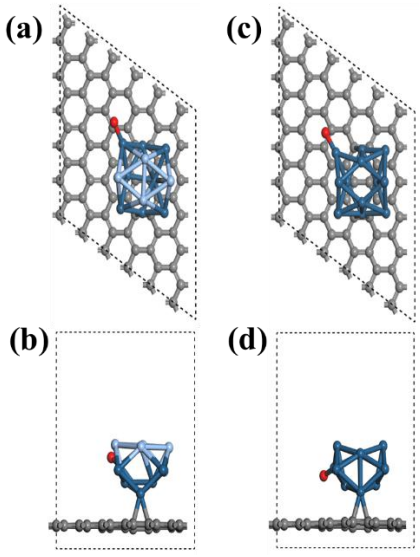

Figure S15. Top (a) and side (b) view of the model of Pt_8Ag_4/ CNT; and top (c) and side (d) view of the model of Pt/CNT and the O atom adsorbed at the optimum site. Dark blue, sky blue, grey and red atoms represent Pt, Ag, C and O, respectively.

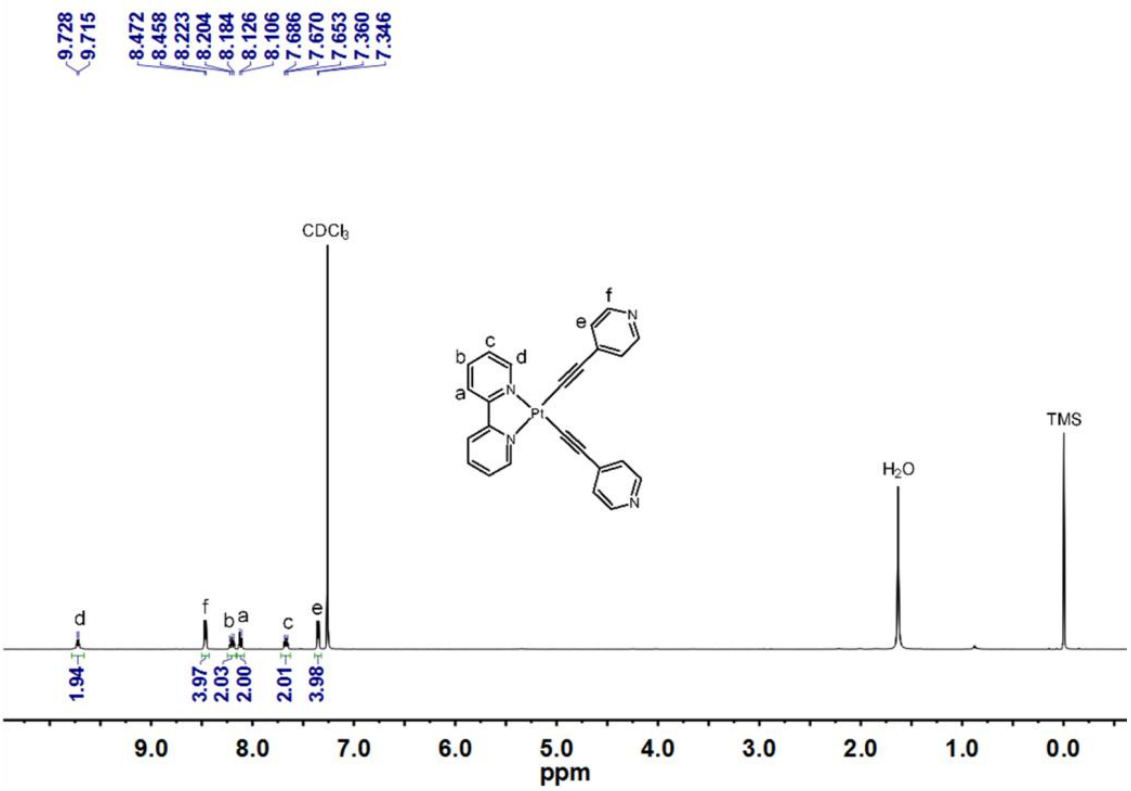

Figure S16. ^{1}H NMR spectrum of Pt metalloligand (400 MHz, $CDCl_3$, 298 K).

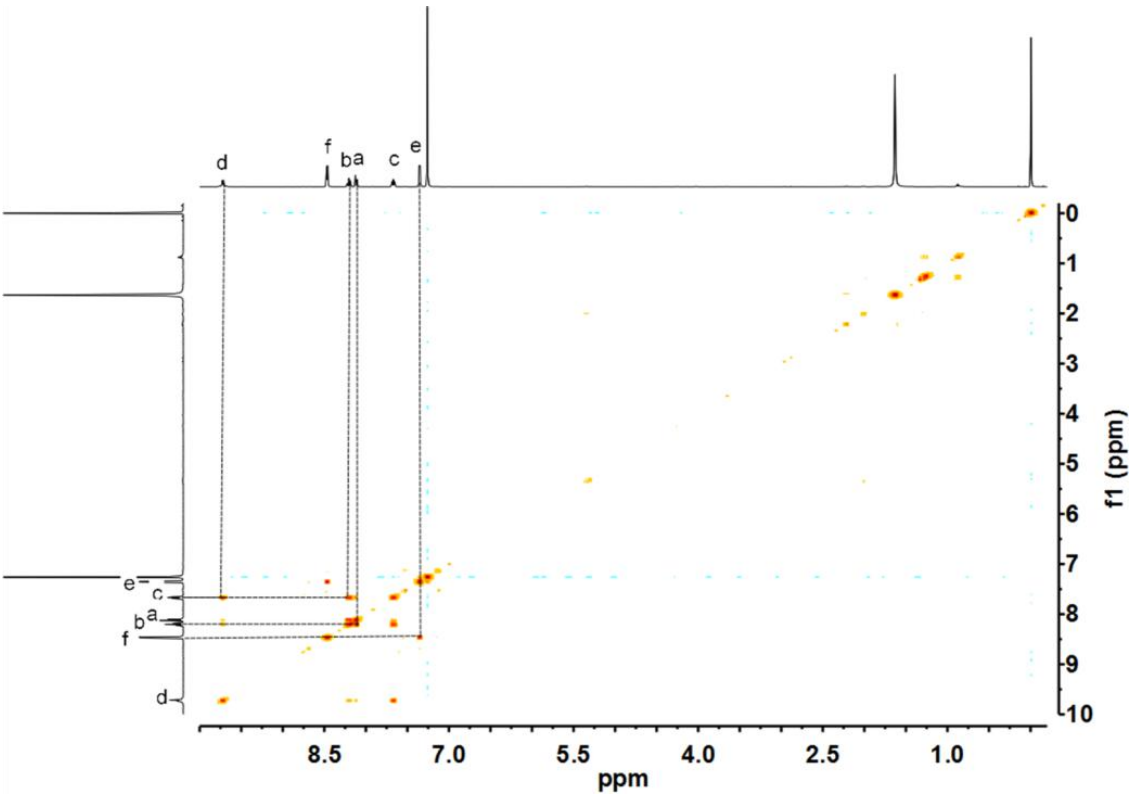

Figure S17. ^{1}H COSY spectrum of Pt metalloligand (400 MHz, $CDCl_3$, 298 K).

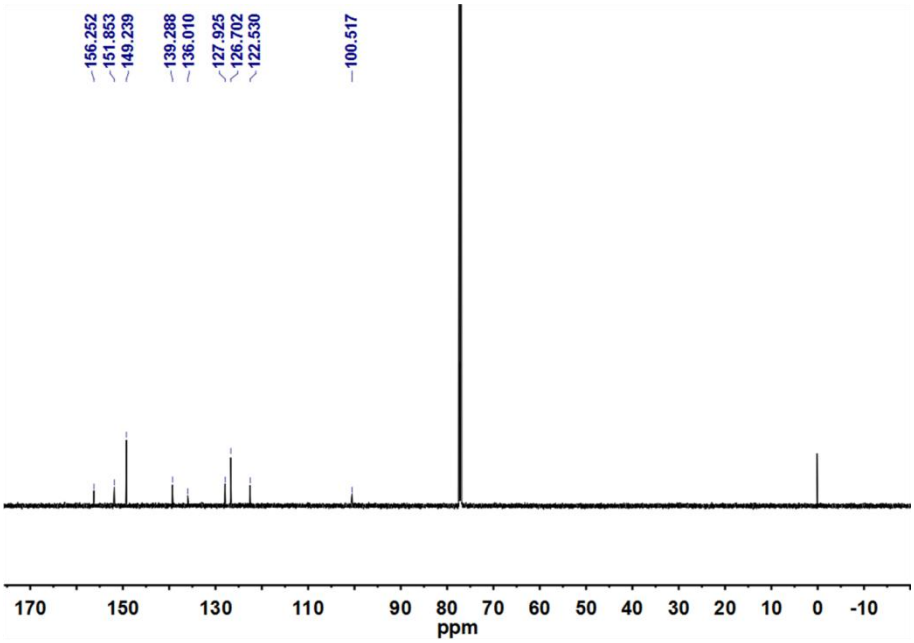

Figure S18. ^{13}C NMR spectrum of Pt metalloligand (100 MHz, $CDCl_3$, 298 K).

Table S1 ICP-MS comparison of Pt_8Ag_4-clusters/CNTs and Pt/CNTs nanostructures.

Samples	**Pt (mg L^{-1})**	**Ag(mg L^{-1})**
Pt_8Ag_4-clusters/CNTs	96.63	23.49
Pt/CNTs	163.22	-

Table S2. Pt L_3-edge white line.

Samples	**E_0 (eV)**	**E_{peak} (ev)**	**△A**
Pt foil	111564	11565.50	6.78
Pt/CNTs	11564.58	11567.19	6.81
Pt_8Ag_4-clusters /CNTs	11564.97	11567.06	6.81
PtAg-MOCs/CNTs	11565.50	11568.54	6.82
PtAg alloy	11563.98	11562.12	8.04
PtO_2	11566.85	11568.39	10.07

Table S3. Summary of electrochemical results of all samples and Pt/C catalysts for HER tested in 0.5 M H_2SO_4 solution.Table Caption.

Samples	E_{onset} (mV) (j=1 mA cm^{-2})	E_{op} (mV) (j=10 mA cm^{-2})	Tafel slope (mV dec^{-1})	TOF (s^{-1}) (E = -0.1V vs. RHE)
Pt_8Ag_4-clusters/CNTs	2	18	25.90	6.36
PtAg-MOCs/CNTs	5	101	22.08	0.60
Pt_8Ag_4-clusters	57	78	34.41	1.40
PtAg-MOCs	80	217	33.69	0.10
Pt/CNTs	57	128	102.72	0.29
PtMLs/CNTs	80	408	67.60	0.015
CNTs	341	432	-	-
Pt/C (20 wt%)	56	77	35.00	2.20

Table S4. Summary of electrochemical results of all samples and Pt/C catalysts for double-layer capacitance (C_{dl}), electrochemical active surface area (ECAS), specific area (SA) and Pt mass activity (MA) in 0.5 M H_2SO_4 solution.

Samples	C_{dl} (mF cm^{-2})	ECSA (cm^{-2})	SA(uA cm^{-2})	MA(A mg_{Pt}^{-1})
Pt_8Ag_4-clusters/CNTs	4.6	131.43	35.0	113.20
Pt_8Ag_4-MOCs/CNTs	1.47	42.00	6.4	6.64
Pt_8Ag_4-clusters	0.4274	12.21	31.3	9.42
Pt_8Ag_4-MOFs	0.395	11.29	4.6	1.27
Pt/CNTs	1.35	38.57	8.2	4.62
PtMLs/CNTs	0.82	23.43	0.6	0.19
CNTs	2.11	60.29	-	-
Pt/C	3.04	86.86	12.6	20.84

Table S5. Impedance components determined by fitting the experimental data using the equivalent circuit.

Samples	R_S	W_s-R	W_s-T	W_s-P	R_{ct}	CPE-T	CPE-P
Pt_8Ag_4-clusters/CNTs	9.142	26.62	0.0205	0.4609	-	-	-
Pt_8Ag_4-MOCs/CNTs	7.313	126.6	0.0511	0.49552	18.84	$6.34*10^{-5}$	0.6922
Pt_8Ag_4-clusters	22.22	-	-	-	108.7	$5.65*10^{-6}$	0.7994
Pt_8Ag_4-MOCs	22.75	-	-	-	308.6	$1.86*10^{-5}$	0.8159
Pt/CNTs	12.56	-	-		54.58	$1.03*10^{-4}$	0.8106
PtMLs/CNTs	14.8	-	-	-	215.9	$8.62*10^{-5}$	0.8739
CNTs	24.9	-	-	-	874.4	$1.04*10^{-4}$	0.9062

R_s represent electrolyte resistance; R_{ct} the charge transfer resistance; CPE represent interfacial resistance

Table S6. Summary of electrochemical results of all samples and Pt/C catalysts for HER tested in 1 M KOH solution.

Samples	E_{onset} (mV) (j=1 mA cm^{-2})	E_{op} (mV) (j=10 mA cm^{-2})	Tafel slope (mV dec^{-1})	TOF (s^{-1}) (E= -0.1V vs. RHE)
Pt_8Ag_4-clusters /CNTs	10	63	51.0	12.71
Pt_8Ag_4-MOCs/CNTs	9	141	3156	-

Pt_8Ag_4-clusters	24	143	86.20	-
Pt_8Ag_4-MOCs	21	126	53.00	-
Pt/CNTs	68	390	41.41	0.43
PtMLs/CNTs	154	469	55.54	-
CNTs	457	-	-	-
Pt/C (20 wt%)	18	86	42	4.425

Table S7. Summary of electrochemical results of all samples and Pt/C catalysts for HER tested in 1 M PBS solution.

Samples	E_{onset} (mV) (j=1 mA cm^{-2})	E_{op} (mV) (j=10 mA cm^{-2})	Tafel slope (mV dec^{-1})	TOF (s^{-1}) (E= -0.1V vs. RHE)
Pt_8Ag_4-clusters /CNTs	78	216	39.00	0.11
Pt_8Ag_4-MOFs/CNTs	81	291	52.12	0.093
Pt_8Ag_4-clusters	121	269	75.8	0.035
Pt_8Ag_4-MOFs	89	285	72.18	0.083
Pt/CNTs	288	463	49.4	0.025
PtMLs/CNTs	426	-	286.8	0.002
CNTs	351	-	-	-
Pt/C (20 wt%)	35	254	43.00	0.32

Table S8. Summary of electrochemical results of all samples and Pt/C catalysts for ORR tested in 0.5 M H_2SO_4 solution.

Samples	E_{onset} (V) (j=0.1 mA cm^{-2})	$E_{1/2}$ (V)	J_K (E=0.3V vs. RHE)	n
Pt_8Ag_4-clusters /CNTs	0.905	0.74	6.58	~4.0
Pt/CNTs	0.714	0.53	1.81	~3.8
Pt/C	0.896	0.657	4.13	-

Table S9. Summary of electrochemical results of all samples and Pt/C catalysts for ORR tested in 0.1 M KOH solution.

Samples	E_{onset} (mV)	$E_{1/2}$ (mV)	J_K	n
Pt_8Ag_4-clusters/CNTs	0.966	0.816	6.48	3.97
Pt/CNTs	0.848	0.675	2.88	~3.00
Pt/C	0.934	0.799	4.35	-

EXPERIMENTAL PROCEDURES

1. Materials

All chemicals and solvents were purchased from Adamas Reagent, Ltd and used without further purification. Anhydrous solvents were distilled according to standard procedures.

Table S10. The details of all Chemicals and solutions.

Chemicals and solvents	Purity(%)	commercial company
dipotassiumtetrachloroplatinate	98	Adamas
2,2'-bipyridine	99	Adamas
4-ethynylpyridine hydrochloride	98	Adamas
Copper(I) Iodide	99	Adamas
4-ethynylpyridine	98	Adamas

hydrochloride

2. Synthesis and characterization of materials

Preparation of Pt metalloligand, Pt-MLs/CNTs and Pt/CNTs

The Pt metalloligand (Scheme S1) was synthesized from standard CuI-catalyzed coupling reactions between the (bpy)PtCl2 precursor (bpy=2,2'-bipyridine) and 4-ethynylpyridine in the presence of triethylamine in dichloromethaneat room temperature, according to the literature protocol. [1] ^{1}H NMR (400 MHz, $CDCl_3$) δ 9.72 (d, J = 5.4 Hz, 2H), 8.47 (d, J = 5.6 Hz, 4H), 8.20 (t, J = 7.8 Hz, 2H), 8.12 (d, J = 8.0 Hz, 2H), 7.67 (t, J = 6.6 Hz, 2H), 7.35 (d, J = 5.5 Hz, 4H). ^{13}C NMR (100 MHz, $CDCl_3$) δ 156.25, 151.85, 149.24, 139.29, 136.01, 127.92, 126.70, 122.53, 100.52. (Figure S16-18)

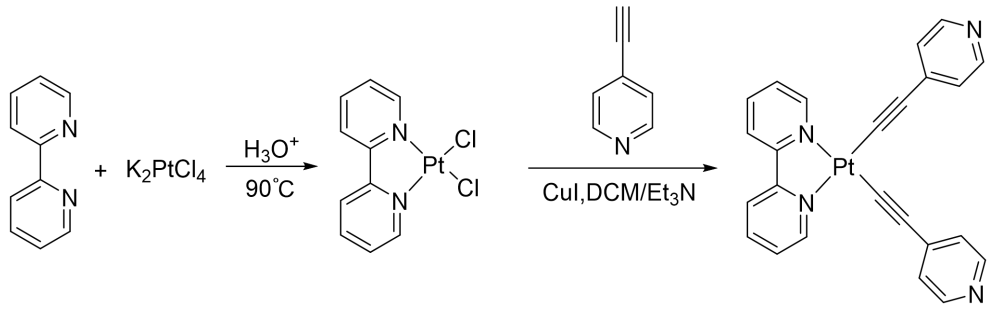

Scheme S1. Synthetic route of Pt metalloligands.

The Pt metalloligand (5 mg) and carbon nanotubes (CNTs, 15 mg) were dissolved in 8 mL of mixed solution [0.48 mL of Nafion (5%), 1.6 mL of ethanol and 5.92 mL of deionized water]. The suspension system was evenly mixed by ultrasonication treatment for 1 h to obtain the stock solution of PtMLs/CNTs.

6.0 μL of the above PtMLs/CNTs stock solution is dripped onto the glassy carbon electrode or rotating disk electrode, and dried by infrared lamp. Then the electrochemical reduction was carried out in sulfuric acid solution (0.5 M) at the voltage of -0.5 V (vs. Ag/AgCl) to prepare the Pt/CNTs for the control experiment.

Preparation of Pt_8Ag_4-MOCs, Pt_8Ag_4-MOCs/CNTs and Pt_8Ag_4-clusters/CNTs.

2 mL of Pt metalloligand (3.3 mg, 0.006 mM) in DCM was added into a glass tube, and 0.5 mL of mixed DCM/CH3OH solvent (v/v=10/1) was added onto it, then 2 mL of $AgBF_4$ (0.6 mg, 0.003 mM) in methanol was dropped on the above solvent slowly.

After a week reaction in dark, orange crystals of Pt_8Ag_4-MOCs were produced (1.17 mg, 30% yield).

5.0 mg of PtAg-MOCs was dispersed in 8 mL of a mixed solution [0.48 mL of Nafion (5%), 1.6 mL of ethanol and 5.92 mL of deionized water]. The suspension was evenly mixed by ultrasonication treatment to prepare the stock solution of Pt_8Ag_4-MOCs/CNTs.

6.0 μL of the Pt_8Ag_4-MOCs/CNTs stock solution was dropped onto the glassy carbon electrode or rotating disk electrode, and dried by infrared lamp. Then the electrochemical reduction was carried out in sulfuric acid solution (0.5 M) at the voltage of -0.5 V (vs. Ag/AgCl) to prepare Pt_8Ag_4-clusters/CNTs.

Materials characterization: The X-ray diffraction (XRD) studies were carried out on Bruker D8 VENTURE photon II diffractometer with Iμs 3.0 microfocus X-ray source using APEX III program. [2] Data reduction was performed with the saint and SADABS package. The structure was solved by direct method and refined by full-matrix least-squares on F^2 with anisotropic displacement using the SHELX software package. [3] Solvent molecules were highly disordered and could not be reasonably located. These residual intensities were removed by a PLATON/SQUEEZE routine. [4]

Table S11. Crystal data and structure refinement for Pt_8Ag_4-**MOCs**.

Identification code	**Pt_8Ag_4-MOCs**
Empirical formula	$C_{194}\ H_{132}\ Ag_4\ B_4\ Cl_4\ F_{16}\ N_{32}\ Pt_8$
Formula weight	5392.55
Temperature	100(2) K
Wavelength	0.71073 Å
Crystal system	Orthorhombic
Space group	Pbca
Unit cell dimensions	a = 25.7770(11) Å
	b = 13.6552(6) Å
	c = 50.9999(19) Å
Volume	17951.5(13) $Å^3$

Z	4
Density (calculated)	1.995 Mg/m^3
Absorption coefficient	6.773 mm^{-1}
F(000)	10256
Crystal size	0.10 x 0.09 x 0.08 mm^3
Theta range for data collection	2.173 to 28.180°.
Index ranges	-30<=h<=34, -18<=k<=15, -67<=l<=64
Reflections collected	122377
Independent reflections	21946 [R(int) = 0.1123]
Completeness to theta = 25.242°	99.9 %
Absorption correction	None
Refinement method	Full-matrix least-squares on F^2
Data / restraints / parameters	21946 / 2315 / 1180
Goodness-of-fit on F^2	1.249
Final R indices [I>2sigma(I)]	R1 = 0.1015, wR2 = 0.1787

The transmission electron microscopy (TEM) and high resolution transmission electron microscopy (HRTEM) images were measured in a JEOL model JEM 2010 EX instrument at an accelerating voltage of 200 kV. The powder was supported on a carbon film coated on a fine-mesh copper grid (3 mm in diameter). The sample suspension in ethanol was sonicated and a drop was dripped on the support film. X-ray photoelectron spectroscopy (XPS) measurements were performed on a PHI Quantum 2000 XPS system (PHI, USA) with a monochromatic Al Kα source and a charge neutralizer. All the binding energy is reference to C 1s peak observed in the XPS spectrum of pure porous carbon.

X-ray absorption fine structure (XAFS) measurements: XAFS data of Pt L_3-edge were collected at BL14W1 station in SSRF and 1W1B station in BSRF. The storage rings of SSRF and BSRF were operated at 3.5 GeV with the current of 300 mA and at 2.5 GeV with the current of 250 mA respectively. The XAFS data were recorded in a transmission mode and then were processed according to the standard procedures using ATHENA module implemented in the IFEFFIT software packages. The L_3-weighted EXAFS spectra were obtained by subtracting the post-edge background

from the overall absorption and normalizing with respect to the edge-jump step. Subsequently, by using a hanning windows (dk=1.0$Å^{-1}$), L_3-weighted χ(k) data in the k-space ranging from 2.4-14.0 $Å^{-1}$ were Fourier transformed to real (R) space that separate the EXAFS contribution from different coordination shells.

3. Electrochemical measurements

Electrochemical measurements were conducted at room temperature (25 °C) on a CHI760E electrochemical workstation (CH instrument Co.) in a three-electrode cell. The carbon electrode and an Ag/AgCl electrode (saturated KCl) are used as the counter electrode and reference electrode, respectively. A glassy carbon electrode (GC) and rotating disk electrode (RDE) with a glassy carbon disk (3.0 mm diameter) served as the substrate for the working electrode. Experimentally, for Pt/C (20 wt%) sample, 2.5 mg of the commercial Pt/C and 7.5 mg of MWCNTs were ultrasonically dispersed in a solution (8 mL) containing 0.05wt% of Nafion (480 μL) and ethanol (1600 μL) for 60 min to form a concentration of 1.25 mg mL-1 catalyst ink. The volumes of catalyst ink were 6 μL for the GC and RDE tests in acid, neutral and alkaline conditions.

The ECSA of a catalyst sample is calculated based on the double layer capacitance according to **Eq. 1**:

$$ECSA = C_{dl}/C_s \qquad (Eq.1)$$

where C_s is the specific capacitance of the sample or the capacitance of an atomically smooth planar surface of the material per unit area in the same electrolyte. For our studying, we use general specific capacitances of C_s = 0.035 mF cm^{-2} in H_2SO_4 based on typical reported values. [5]

The oxygen reduction reaction test is as follows. In alkaline conditions, the RDE tests were carried out in an O_2-saturated 0.1 M KOH solution. In acidic condition, the RDE tests were carried out in an O_2-saturated 0.5 M H_2SO_4 solution. The scan rate was 50 mV s^{-1} for CV measurements and 5 mV s^{-1} for the RDE tests.

The electrocatalysis studies for hydrogen evolution reaction test are conducted as follows. In alkaline conditions, the GC tests were carried out in 1 M KOH solution. In neutral condition, the GC tests were carried out in 1 M PBS solution. In acidic condition, the GC tests were carried out in 0.5 M H_2SO_4 solution. The scan rate was 50 mV s^{-1} for CV measurements and 5 mV s^{-1} for the RDE tests.

All the potentials in this study were calibrated with a reversible hydrogen electrode (RHE), and the potential conversion formula as following: [6-7]

$$E_{RHE} = E_{Ag/AgCl} + 0.0591\ V \times pH\ (at\ 25\ °C) \quad (Eq.2)$$

For the RDE tests, the polarization curves were collected at disk rotation from −1.0 V to +0.2. The polarization curves were carried out at a scan rate of 5 mV s^{-1} at different rotation rates ranging from 400 to 2500 rpm. The limited diffusion currents (J_K) and the electron transfer number (n) can be obtained according to the *K-L* plots which based on the Koutecky-Levich (***K-L***) equations [**Eq. (3-5)**]:

$$1/J = 1/J_L + 1/J_K = 1/(BW^{1/2}) + 1/J_K \quad (Eq.3)$$

$$B = 0.2nFC_0(D_0)^{2/3}v^{-1/6} \quad (Eq.4)$$

$$J_K = 1/(nkFC_o) \quad (Eq.5)$$

The constant 0.2 is adopted when the rotation rate is expressed in rpm. For the Tafel plot, the kinetic current was calculated from the mass-transport correction of RDE by:

$$J_K = (J_L * J)/(J_L - J) \quad (Eq.6)$$

where J represents the measured current density; J_K and J_L are the kinetic- and diffusion-limiting current densities, respectively; w is the linear rotation speed (rpm s^{-1}) of the disk; F is the Faraday constant ($F=96485\ C\ mol^{-1}$), C_0 is the bulk concentration of O_2 ($C_0=1.2*10^{-6}\ mol\ cm^{-3}$), D_0 is the diffusion coefficient of O_2 in 0.1M KOH solution ($D_0=1.9*10^{-5}\ cm^2/s$), v is the kinematic viscosity of the electrolyte ($v=0.01\ cm^2\ s^{-1}$), and k is the electron-transfer rate constant.

The stability test was performed at a static potential at room temperature with the working electrode rotating at 1600 rmp in O_2-saturated solution for ORR studying. The stability test was performed at a static potential (0.24 V vs Ag/AgCl) at room temperature for HER and the chronomperometry test was performed at a static current density (10 mA cm^{-2}) in 0.5 M H_2SO_4 solution.

The TOF (s^{-1}) can be calulated with the following equation: [8]

$$TOF = I/(2Fn_a) \quad (Eq.7)$$

Q is the voltannmentric charge; F is the Faraday constant (96485 mol^{-1}); I is the current (A) during the linear sweep measurement; n_a is the number of active sites (mol).

4. The Calculation Method of Density Functional Theory (DFT) Calculation Method

DFT calculations were performed with periodic super-cells under the generalized gradient approximation (GGA) using the Perdew-Burke-Ernzerhof (PBE) function for exchange-correlation and the ultrasoft pseudopotentials for nuclei and core electrons. The Kohn-Sham orbitals were expanded in a plane-wave basis set with a kinetic energy cutoff of 30 Ry and the charge-density cutoff of 300 Ry. The Fermi-surface effects have been treated by the smearing technique of Methfessel and Paxton, using a smearing parameter of 0.02 Ry. The Brillouin-zones were sampled with a k-point mesh of 3×3×1. The vacuum layer was ~15 Å to remove the slab interaction between the z direction. The models of Pt8Ag4/CNT and Pt/CNT have been relaxed before calculated to optimize the structure. The DFT calculations are given by the PW module contained in the Quantum ESPRESSO distribution.[9]

REFERENCES

1. Whittle CE, Weinstein JA, George MW, Schanze KS. Photophysics of diimine platinum (II) bis-acetylide complexes. Inorganic chemistry. 2001; 40(16):4053-4062.
2. APEX III, Data collection software (version 2017.3)
3. Sheldrick GM. A short history of SHELX. Acta Crystallographica Section A: Foundations of Crystallography. 2008; 64(1):112-22.
4 Spek AL. Single-crystal structure validation with the program PLATON. Journal of applied crystallography. 2003; 36(1):7-13.
5. McCrory CC, Jung S, Ferrer IM, Chatman SM, Peters JC, Jaramillo TF. Benchmarking hydrogen evolving reaction and oxygen evolving reaction electrocatalysts for solar water splitting devices. Journal of the American Chemical Society. 2015; 137(13):4347-57.
6. Liu L, Ci S, Bi L, Jia J, Wen Z. Three-dimensional nanoarchitectures of Co nanoparticles inlayed on N-doped macroporous carbon as bifunctional electrocatalysts for glucose fuel cells. Journal of Materials Chemistry A. 2017; 5(28):14763-74.

7. Ye L, Chai G, Wen Z. Zn-MOF-74 derived N-doped mesoporous carbon as pH-universal electrocatalyst for oxygen reduction reaction. Advanced Functional Materials. 2017; 27(14):1606190.
8. Wang J, Xu F, Jin H, Chen Y, Wang Y. Non-noble metal-based carbon composites in hydrogen evolution reaction: fundamentals to applications. Advanced materials. 2017; 29(14):1605838.
9. Giannozzi P, Baroni S, Bonini N, et al. QUANTUM ESPRESSO: a modular and open-source software project for quantum simulations of materials. Journal of physics: Condensed matter. 2009; 21(39):395502.